V -

TRNL-77/1-Ph

Direct Measurement of Prompt Neutrons Emitted in Fission of ^{226}Ra by 12 MeV Protons

A. Gayer and Z. Fraenkel

Weizmann Institute of Science

Rehovot Israel

Abstract

Prompt neutron energy distributions were measured at 0° and 90° with respect to the fission axis, in correlation with the mass-energy distribution of the fragments, for the fission of ^{226}Ra induced by 12 MeV protons. The average number and average kinetic energy of prefission and postfission neutrons were obtained as a function of fragment mass and total kinetic energy. The average number of prefission neutrons emitted is 0.33±0.15 n/fission (this includes also contributions from scission neutrons). By comparing this result with calculations of the average number of "true" prefission neutrons, it was found that the number of "true" prefission neutrons is zero. The average number of postfission neutrons emitted from both fragments is 3.20±0.20 with an average kinetic energy of 1.33±0.07 MeV. The dependence of the number of postfission neutrons on the fragment mass can be interpreted as a combination of a saw-tooth structure for the asymmetric mass division and a linearly increasing function for the symmetric mass division.

NUCLEAR REACTIONS, FISSION ^{226}Ra (p,xnf), E=12 MeV; measured coin fragment energy, neutron velocity at θ = 0°, 90° with respect to fragment; deduced number and kinetic energy of pre-fission, post-fission neutrons.

I. Introduction

The characteristics of fission of ^{226}Ra by projectiles of moderate energies have raised considerable interest, because they seem to be a combination of the characteristics of fission of light nuclei and low-excitation fission of heavy nuclei. Jensen and Fairhall[1] who first measured the triple-peaked mass distribution for the fission of ^{226}Ra by 11 MeV protons, suggested that the asymmetric peaks result from low excitation fission of the residual nucleus which is left after emission of a neutron by the compound nucleus, whereas the symmetric peak results from the primary fission of the compound nucleus, corresponding to high-excitation fission. This possibility was excluded by Konecny et al.[2] and Weber et al.[3] who obtained triple-peaked mass distribution at low excitation fission of Ac and Ra isotopes, where second-chance fission is energetically forbidden. This result is also confirmed by the present work. It seems therefore that both fission modes originate in the same nucleus, and according to Ref. (3) pass through different saddle points.

A very interesting feature of the fission of Ra is the dependence of the number of post-fission neutrons on the fragment mass. Konecny and Schmitt[4] obtained the number of neutrons emitted by the fragments, for the fission of ^{226}Ra by 13 MeV protons by an indirect method and their results are consistent with a two-component interpretation. A direct measurement of the prompt neutrons emitted in fission of ^{226}Ra by 16 MeV protons, was recently made by Fraenkel et al[5]. But the mass distribution in their results is almost entirely symmetric and therefore the dependence of the number of post-fission neutrons on

the fragment mass resembles that obtained for symmetric fission.

In this paper we describe an experiment in which we measured directly the number of prompt neutrons and their energies in correlation with the fragment mass and kinetic energy, for the fission of ^{226}Ra by 12 MeV protons. For that energy the mass distribution is triple-peaked, with almost equal contributions of the symmetric and asymmetric components, which allows a better comparison to be made between the two fission modes. The neutrons were measured by the time-of-flight method at 0° and 90° to the fission axis. This enables us (with certain assumptions to be discussed below) the determination of the number and energy spectrum of the prefission neutrons, as well as the number and the energy spectrum of the postfission neutrons.

The experimental technique will be presented in the next section, and in Sec. III the data analysis will be described. In Sections IV and V we present the results for the pre- and postfission neutrons, and discuss them in terms of the two-mode interpretation.

II. Experimental Method

A. General

A thin target of ^{226}Ra was bombarded by a beam of 12 MeV protons, from the Weizmann Institute Tandem Van-de-Graaff acceierator. The fission fragment energies were measured by two pairs of solid state detectors, and the neutron velocities were measured by the time-of-flight method. The start pulse for the time measurement was given by one of the fission detectors in each pair, and the stop pulse by the neutron detector. The neutrons were detected by two neutron detectors at 0° and 90° to the fission axis, and the separation between the prefission

and postfission neutron spectra was performed by an iterative procedure described in the next section.

Binary events, consisting of two fragment energies, and triple events consisting of two fragment energies and a neutron or gamma flight time were stored on magnetic tape in chronological order with the aid of an on-line PDP-9 computer. A similar experiment was made with a ^{252}Cf source, in order to calibrate the fission detectors, and to obtain the efficiency of the neutron detectors.

B. Experimental Arrangement

The scattering chamber was especially designed, in order to reduce the effect of neutron scattering from the walls. Its shape was that of a cylinder of 25 cm diameter and 3 mm thickness with a semi-spherical top of 2 mm thickness. Two target holders, one for the ^{226}Ra target and one for the ^{252}Cf source, were in the plane normal to the beam direction, and at 45° to the horizontal plane. The Ra target was rotated by 45° with respect to the plane normal to the beam direction.

The geometrical arrangement of the detectors is shown in Fig. 1. In order to increase the counting rate, two pairs of fission fragment detectors were used. They were arranged in the plane normal to the beam direction and at 90° to each other. The fission fragment detectors were surface-barrier detectors, with an active area of 4 cm^2. One detector in each pair (F1,F3) was at a distance of 6.9 cm from the center of the target whereas the other one (F2,F4) was at a distance of 5 cm. In this way we obtained a coincidence efficiency of 85%. The detectors were covered with 100 $\mu g/cm^2$ Ni foils as a protection against low-energy radiation.

The neutrons were detected by two scintillators mounted on 58 AVP photomultipliers (denoted PM1 and PM2 in Fig. 1). Two types of scintillators were used during the experiment: a plastic scintillator (NE 102), which is a fast scintillator and is suitable for obtaining good time resolution, and a liquid scintillator (NE 213) which has good pulse shape discrimination properties. The scintillators were of 2" length and 5" diameter, and were mounted outside the chamber at a distance of 42 cm from the center of the target. Each detector was colinear with one pair of fission fragment detectors. The neutron detectors were shielded by 1 cm of lead, in order to reduce the number of random events (due to γ rays emitted from the collimators and backing), and the effect of (n,γ), $(n,n'\gamma)$ reactions in the chamber walls.

The Ra target consisted of about 50 $\mu g/cm^2$ ^{226}Ra evaporated on a 20 $\mu g/cm^2$ carbon backing.*) We used a ^{252}Cf source of $\sim 10^6$ fission/minute deposited on a 100 $\mu g/cm^2$ Ni backing, for calibration.

C. Electronic System and Data Collection

The electronic system was designed to measure two types of events: binary events, which consisted of two fission fragments detected by detectors F1,F2 or F3,F4 and triple events which consisted of two fission fragments and a neutron detected by PM1 or PM2. The electronic system consisted of standard fast-slow techniques, and is described schematically in Fig. 2. The discrimination level of the time pick-off units following the fission fragment detectors, was set just above the

*) We are deeply grateful to Prof. H.J. Specht and Dr. E. Konecny for the preparation of the Ra targets.

pulse height of 7.7 MeV alpha particles from ^{212}Po in the ^{226}Ra chain. The photomultipliers threshold was controlled by the Ortec 403A unit, which permitted the rejection of low-pulse-height events. The discrimination level was set at half the Compton edge of ^{241}Am, which is equivalent to a neutron energy of 200 keV.

When using the liquid scintillator NE-213, we measured, in addition to the fast photomultipler signal, the risetime of the linear signal, which was converted to an analog pulse by an Ortec pulse-shape-analyser unit after amplification by a DDL amplifier.

Calibration measurements with the ^{252}Cf source were performed with the same experimental setting. In this way we obtained the calibration constants for the energy measurement of the fragments and the neutron detection efficiency.

A total of 3.5×10^{6} binary events and 1.8×10^{5} triple events were obtained in the Ra experiment, with an average proton current of 120 nA.

III. Data Analysis

A. Primary Analysis

The raw data were first analysed in order to obtain the masses and kinetic energies of the fission fragments and the time-of-flight of the neutrons or gammas.

The masses and kinetic energies were determined by an iterative procedure using the calibration formula of Schmitt et al.[6]. The calibration constants were obtained from an identical experiment done with a ^{252}Cf source. The average number of neutrons $\bar{\nu}(A,E_K)$ used for the neutron correction in the Ra experiment, was taken from our own results, after a preliminary analysis made by using the results of

Konecny et al.[4]. Corrections for energy loss in the target and backing were made in each iteration with the relation given by Alexander and Gazdick[7].

The mass-energy yield was obtained with the above procedure by considering all the events as binary events. In analysing triple events, the fragment masses and kinetic energies were corrected for the recoil of the detected neutron[8].

The neutron time-of-flight was obtained by a procedure similar to that described in Ref. 5, which includes corrections for the time-of-flight of the fission fragment, and the "walk" in the time determination by the solid state detector.

The time-of-flight spectrum at 0° and 90° with respect to the fission axis is shown in Fig. 3. The width of the γ peak was 1.8 nsec FWHM, and its height was considerably reduced by the lead shielding of the scintillators. A good separation between neutrons and gammas was obtained at 0°, whereas the separation at 90° was not quite as good. In order to improve the separation between neutrons and gammas, and especially those gammas which result from (n,γ), $(n,n'\gamma)$ reactions, we used liquid scintillators which have good pulse shape discrimination properties. A typical rise-time distribution obtained in our experiment is shown in Fig. 4. The combined use of the time-of-flight spectrum and pulse shape analysis, improved the separation between neutrons and gammas by 12% at 90° (i.e. 12% of the events in the neutron time-of-flight distribution were determined to be gammas). However, this did not affect the final results since we used an effective efficiency for the neutron detectors as will be discussed later.

B. Neutron Detection Efficiency

The efficiency of the neutron detectors as a function of the neutron velocity $\varepsilon(v)$, was obtained by measuring the neutron spectrum of ^{252}Cf, and comparing it to the absolute results of Bowman et al.[9]. $\varepsilon(v)$ was calculated with the correction of Bowman's results for the finite size of the detectors and extrapolation to the angles in our experiment, as described by Gavron et al.[10]. Our results of $\varepsilon(v)$ for 0° and 90° to the fission axis are shown in Fig. 5, together with the theoretical efficiency, calculated with the assumption of single scattering of the neutrons in the scintillator. The structure observed in the theoretical efficiency is due to resonances in the scattering of neutrons by carbon at these energies. The experimental efficiency at 90° is higher than at 0° for velocities up to 2.5 cm/nsec (~3 MeV). This is probably due to higher relative contributions of scattered neutrons from the surrounding material. Comparing the experimental values to the calculated efficiency, which is the intrinsic efficiency of the scintillator, we see that the effect of neutron scattering is very small for 0°. For higher velocities the experimental efficiency for both angles rises above the calculated efficiency, which presumably is due to the (n,γ) and $(n,n'\gamma)$ reactions in the walls of the chamber. This effect was much stronger when we performed the same experiment without the lead shielding around the scintillators, whereas the efficiency at lower velocities was not affected by it. Without the lead shielding the efficiencies at 0° and 90° were almost equal at high velocities. The reason for this difference is not obvious.

The efficiency obtained for ^{252}Cf was used without modification in analyzing the results of the ^{226}Ra experiment, because of the similarity of the angular and energy distribution of the neutrons emitted in the two cases. In this way the neutron results were corrected for scattering and (n,γ), $(n,n'\gamma)$ contributions to first order. The fact that the neutron results were not affected by the use of the pulse shape discrimination method, which reduced the contribution of inelastic reactions, indicates that the effective efficiency used, takes into account reasonably well these effects.

C. Postfission and Prefission Neutrons

The experimental neutron spectrum may be divided into the following components: (1) Prefission neutrons emitted from the compound nucleus before fission. (2) Scission neutrons believed to be emitted during the fission process - between saddle - and scission points. (3) Postfission neutrons emitted from the fission fragments.

The number and energy distribution of the prefission and postfission neutrons were obtained from the experimental angular and energy distribution, on the basis of two assumptions: (1) The prefission and scission neutrons are emitted isotropically in the laboratory frame (neglecting the recoil momentum of the fissioning nucleus). (2) The postfission neutrons are emitted from the fully accelerated fragments with an isotropic angular distribution in the fragment frame.

No assumptions were made regarding the shape of the neutron energy spectrum, except that we were restricted experimentally to the energy range of 0.5-10.0 MeV in the laboratory system. Since the same angular distribution is assumed for the prefission and scission

neutrons, they cannot be separated in our analysis, and in the following the term prefission neutrons will include both components. A more detailed discussion and justification of the above assumptions is given in Section V.

The number and energy distribution of the prefission neutrons $\bar{\nu}_b(A,E_k)$ and $\bar{\eta}_b(A,E_k)$ respectively, and the corresponding distributions for the postfission neutrons $\bar{\nu}_a(A,E_k)$ and $\bar{\eta}_a(A,E_k)$ were determined by an iterative procedure similar to that of Cheifetz et al.[11]. The following modifications were made in our analysis: (1) The analysis was made event by event, by calculating the contribution of each event to ν_a , η_a and ν_b , η_b according to the equations of reference[11], and normalized by the effective efficiency of the neutron detector. (2) The fragment masses and kinetic energies were corrected for the recoil of detected neutrons, according to Gavron[8]. A detailed description of the iteration method is given in Ref. (5). By this method we obtained upper and lower limits to the values of $\bar{\nu}$ and $\bar{\eta}$, and the results which are reported below are the averages of those limits obtained after one iteration.

D. Random Events

The random events were due to gammas and neutrons emitted from the target backing, collimators and beam stop, and gammas emitted from the ^{226}Ra target and its daughters. The collimators were shielded with lead, and the beam stop was at a distance of 7 m from the target chamber and was also shielded by concrete wall in order to reduce the number of random events. A further reduction by 50% resulted from the

use of the pulse shape discrimination method

The random spectrum was obtained by detecting those events in which the "stop" signal preceded the "start" signal of the fission fragment. The random spectrum was constant in time, as expected, and amounted to 13% and 3% of the total number of true events at 90° and 0°, respectively. They were subtracted event by event during the analysis described in Section III.C.

IV. Experimental Results

A. Mass-Energy Yield

The fission yield $Y(A,E_k)$ is represented in Fig. 6 as a contour plot of counts vs. fragment mass and total kinetic energy before neutron emission. This plot was obtained by considering all the fission events as binary events, and ignoring neutron detection. The results were not corrected for dispersion effects, since these were found to be negligible for the mass-energy yield[12]. The mass-energy yield is a triple peaked distribution, in which one peak is centered at symmetric mass divisions, and the other two are located at asymmetric mass divisions with higher total kinetic energy. Projections of $Y(A,E_k)$ on the mass and energy axes, are shown by the full lines in Fig. 7 and 8 respectively. By comparing the mass yield shown in Fig. 7 with those obtained at other excitation energies[1,4,13], we see that the ratio of the symmetric to asymmetric fission yield for our results, is consistent with the trend of increasing symmetry with excitation energy. The total kinetic energy distribution shown in Fig. 8 has a most probable value of 155.9±2.0 MeV, and a standard deviation of 10.9 MeV, which are in good agreement with the results of

Ref. 4 and 5, obtained for fission of ^{226}Ra induced by 13 MeV and 16 MeV protons respectively. The uncertainty in the value of the total kinetic energy results mainly from the uncertainty in the target thickness and the constants used for calculating the energy loss in the target according to Ref. 7.

From the mass-energy yield shown in Fig. 6 it follows that for low kinetic energy values, the symmetric mass peak dominates, whereas the asymmetric peaks dominates for high kinetic energies. A good separation between symmetric and asymmetric fission, is obtained by a cut in the mass-energy plane. We have used a parabolic curve, which is shown by a dashed line in Fig. 6. The mass distribution for the two fission modes is shown by full lines in Fig. 16, and is discussed later in connection with the neutron distribution.

B. The Neutron Spectrum in the Laboratory Frame

The neutron energy spectrum in the laboratory system at 0° and 90° to the fission axis, is shown in Fig. 9, together with the corresponding spectra for spontaneous fission of ^{252}Cf, obtained in the calibration experiment. The spectrum at each angle was normalized by the effective efficiency for the corresponding angle which was derived from the ^{252}Cf experiment as discussed previously. Statistical subtraction of random events was applied to the spectra of $^{226}Ra+p$, and this may be the reason for the fluctuations seen in the spectrum at 90° where the number of random events was higher. Table I summarizes the average numbers of neutrons/sr per fission event and average kinetic energy of the neutrons, at 0° and 90° to the fission axis, for fission of $^{226}Ra+p$ and ^{252}Cf as obtained in our experiment,

and by results of Bowman et al.[9] for ^{252}Cf. The similarity of the neutron energy spectra of $^{226}Ra+p$ and ^{252}Cf as is seen in Fig. 9 and the similar values obtained for the ratio $N(0°)/N(90°)$ for the two cases, justifies the use of the effective efficiency of ^{252}Cf for the $^{226}Ra+p$ data.

C. Postfission Neutrons

The average number of postfission neutrons per fragment $\bar{\nu}_a(A,E_k)$, as a function of the fragment mass and total kinetic energy, before neutron emission, is shown in Fig. 10 in the form of a contour diagram. For reference the lowest contour line of the mass-energy contour diagram (Fig. 6) is indicated by a dashed line. We see that the average number of neutrons in the region of the symmetric peak, increases as the total kinetic energy decreases and the fragment mass increases. A similar behaviour was obtained by Plasil et al.[14] for the fission of ^{213}At, which fissions symmetrically. The weighted average number of neutrons as a function of mass $\bar{\nu}_a(A)$, and as a function of total kinetic energy $\bar{\nu}_a(E_k)$, are shown in Fig. 7 and Fig. 8 respectively.

The trend of $\bar{\nu}_a(A)$ seen in Fig. 7 is similar to that obtained by Konecny et al.[4] and Fraenkel et al[5] for the fission of ^{226}Ra by 13 MeV and 16 MeV protons respectively, except for the pronounced dip at mass ∿103 amu observed in our results. The dependence of $\bar{\nu}_a$ on the fragment mass, in connection with the two fission-mode interpretation, will be discussed in greater detail in Section V. The results of $\bar{\nu}_a$ were corrected for neutrons outside the experimental detection limit. This was done by comparing the average total number

of neutrons emitted in the spontaneous fission of ^{252}Cf as obtained in our calibration experiment, to the latest value of 3.725[15] n/fission. Our results for $\bar{\nu}_a(A)$ are lower by about 0.5 neutrons than the results of Ref. (4), which were obtained by an indirect method, namely by subtracting the post-neutron emission mass from the pre-neutron emission mass. This is consistent with the conclusion of Fraenkel et al.[5] that the indirect method yields higher values for $\bar{\nu}_a(A)$ than the direct neutron counting method. The average number of postfission neutrons obtained in our experiment is 1.60±0.10 per fragment.

The average number of neutrons emitted from a single fragment, as a function of the total kinetic energy $\bar{\nu}_a(E_k)$ is shown in Fig. 8, together with the total kinetic energy distribution. $\bar{\nu}_a$ decreases monotonically with increasing total kinetic energy, with a slope of 0.04 n/MeV. This number was obtained by a linear fit to $\bar{\nu}_a(E_k)$. It is much lower than the slope obtained by Konecny et al.[4], since their Schmitt calibration constants were adjusted to reproduce the results of Bowman et al.[9] for ^{252}Cf which, contrary to our analysis, were not corrected for the neutron recoil effect[8].

The average derivative of $\bar{\nu}_a$ with respect to E_k as a function of the fragment mass, is shown in Fig. 11, together with the fragment mass distribution. The behaviour of $\frac{\partial \bar{\nu}_a}{\partial E_k}(A)$ agrees in general with that obtained by Konecny et al.[4], however, the absolute values are lower for the reason mentioned before. In the region of symmetric mass division, $\frac{\partial \bar{\nu}_a}{\partial E_k}$ increases linearly with increasing fragment mass, following a similar trend of $\bar{\nu}_a$. This means that additional excitation energy is distributed between the two fragments according to their

average excitation energy. For asymmetric mass divisions, there seems to be no clear trend of $\frac{\partial \bar{\nu}_a}{\partial E_k}$, especially for the heavy masses.

The separation energy, which is the average energy necessary to emit one additional neutron per fission event, was obtained according to the equation:

$$\overline{SE} = \frac{\sum_{A,E_k} < \frac{\partial \bar{\nu}_T}{\partial E_k}(A,E_k) >^{-1} Y(A,E_k)}{\sum_{A,E_k} Y(A,E_k)} \qquad (1)$$

and is equal to 8.9 MeV/neutron. This is close to the value of 8.6 MeV/neutron obtained by Nifenecker et al.[16] for ^{252}Cf, however, due to the recoil correction, our result is higher than the value of 6.4 MeV/neutron reported in Ref. 4.

One of the advantages of our direct neutron counting method is the possibility to measure the kinetic energy of the neutrons. The postfission neutron spectrum in the c.m. system of the fragment is shown in Fig. 12. It has an approximately Maxwellian shape as predicted by the evaporation theory, and has an average value of $\bar{\eta}_a$ = 1.33±0.07 MeV. The energy distribution has a cutoff at 7.0 MeV, as a result of the experimental upper limit of 10.0 MeV in the laboratory neutron energy. The dependence of the average neutron kinetic energy $\bar{\eta}_a(A)$ on the fragment mass is shown in Fig. 13. $\bar{\eta}_a(A)$ is peaked around mass 132 amu, which corresponds to a double magic nucleus (^{132}Sn), similar to what is found for the spontaneous fission of ^{252}Cf.[10]

D. Prefission Neutrons

As was already discussed in Section III, the "prefission neutrons" obtained by our analysis, are actually the isotropic component (in the laboratory system) of the neutron distribution, which includes the "true" prefission neutrons and the "scission" neutrons. Both have an isotropic angular distribution in the laboratory system. The average number of prefission neutrons per fission event as a function of fragment mass $\bar{\nu}_b(A)$ is shown in Fig. 14. (The distribution is assumed to be symmetric with respect to mass 115.5). Within the experimental error, the number of prefission neutrons is independent of the fragments mass (as expected), and is equal to 0.33±0.15 n/fission. This result is consistent with the result reported in Ref. 5, for the fission of ^{226}Ra by 16 MeV proton, and is close to the value obtained by Bowman et al.[9] for the isotropic component of the neutron distribution in spontaneous fission of ^{252}Cf.

The prefission neutron energy spectrum in the laboratory system which is shown in Fig. 15, is qualitatively similar to the postfission neutron spectrum. However, the average kinetic energy of the prefission neutrons is $\bar{\eta}_b$ = 2.48±0.25 MeV (as compared to $\bar{\eta}_a$ = 1.33±0.07 MeV for the postfission neutrons), and is equal (within the error) to the value of 2.60 MeV obtained by Bowman et al.[9] for the average energy of the isotropic component of the neutron distribution in spontaneous fission of ^{252}Cf. The prefission neutrons have a higher kinetic energy than expected from the evaporation model (1.0-1.5 MeV) at our excitation energy, and their number and energy distributions are close to those for ^{252}Cf. This seems to indicate that they are mostly scission

neutrons, which are emitted during the fission process itself, by a mechanism which differs from statistical evaporation.

V. Discussion

A. Justification of the Assumptions

The neutron analysis assumes isotropic emission of the prefission neutrons in the laboratory system and of the postfission neutrons in the c.m. system of the fragments (see Section III.C). In order to justify these assumptions, the following points have to be checked: (1) The effect of the angular momentum of the fissioning nucleus on the angular distribution of the prefission neutrons. (2) The effect of the angular momentum of the fission fragments on the angular distribution of the postfission neutrons. (3) The possibility of neutron emission from the fragments during the fragment acceleration period.

The angular distribution of the prefission neutrons is peaked in the forward-backward directions with respect to the beam, because of the angular momentum transferred by the projectile. Therefore, the total number of prefission neutrons obtained by our analysis is an underestimate. But in the case of a proton beam of 12 MeV, the anisotropy is expected to be very small, and according to Ericson and Strutinsky[17] is less than 5%, which is within our experimental error. It should be emphasized, that the anisotropy of the prefission neutrons does not affect the determination of the number of the postfission neutrons, since the prefission neutrons distribution is isotropic in the detectors plane, which was perpendicular to the beam direction.

The angular momentum of the fission fragments affects the angular distribution of the postfission neutrons in the fragment c.m. frame, in the same way as for the prefission neutrons. The fragment angular momentum was found to be aligned perpendicular to the fission axis[18]. This causes the neutron distribution to be peaked in the direction of the fission axis, and results in an overestimate of the number of postfission neutrons. Cheifetz et al.[11] estimated the size of this effect, and concluded that the angular momentum of the fission fragments does not affect the results for the postfission neutrons within our experimental error.

Neutron emission before the fragments have achieved their final velocity, will result in an underestimate of the number of postfission neutrons, and an overestimate of the number of prefission neutrons. In order to examine this effect, we used the Monte-Carlo simulation program of Gavron[8]. We generated triple events by having only the first neutron in the evaporation cascade be emitted before the fragments achieved their final velocities. The data so generated was analyzed by the method described in Section III, assuming neutron emission from the fully accelerated fragments. As a result we concluded that the effect of neutron emission before full acceleration of the fragments, for the range of excitation energies gained by the fragments in our experiment, is within our experimental error.

B. Postfission Neutrons

The results for the fission of ^{226}Ra by projectiles of moderate energies, were interpreted by a number of authors (4,19) as a combination of two fission modes. As we already saw in Section IV, a good separation between the symmetric and asymmetric modes is obtained by a cut in the mass-energy plane. In Fig. 16 are shown the postfission neutron distributions for the two modes, as a function of the fragment mass, together with the corresponding mass distributions. For the symmetric mode the average number of neutrons increases linearly with mass (the small dip at mass ~103 is probably due to contribution of the asymmetric mode). This is in agreement with the liquid drop model calculation of Nix and Swiatecki[20], and the experimental results obtained for fission of ^{213}At, which fissions symmetrically[5,14]. The slope $\frac{\partial\bar{\nu}}{\partial A}$ in the symmetric region is 0.05 neutron/amu, in agreement with the value obtained by Fraenkel et al.[5] for ^{213}At, but much higher than the value of 0.02 predicted by the LDM calculations[14]. For the asymmetric mode the neutron distribution has a saw-tooth structure, which is well known from low excitation fission of heavy nuclei. The average number of postfission neutrons for the symmetric mode is 1.85±0.10 neutron/fragment, compared to only 1.35±0.07 neutron/fragment for the asymmetric mode. A similar separation for the kinetic energy distribution of the neutrons, yields almost equal average energies for the two modes. A detailed energy balance calculation including these results and total gamma energies, will be given in the following paper.

C. Prefission Neutrons

The interpretation of the number of prefission neutrons obtained in our experiment suffers from the fact that the number of scission neutrons could not be determined separately. However, their number can be estimated by measuring the isotropic component of the neutron distribution in the spontaneous fission of ^{252}Cf, or in the thermal neutron-induced fission of ^{235}U, where second chance fission is energetically forbidden. This component as determined by Bowman et al.[9], and in our experiment for ^{252}Cf is almost equal to the average number of prefission neutrons for the induced fission of ^{226}Ra by 12 MeV protons. This result may be an indication that almost all prefission neutrons obtained by us are scission neutrons. This conclusion is supported by the fact that the average kinetic energy of the prefission neutrons is much higher than the average energies of 1.0-1.5 MeV expected for the evaporation neutrons emitted from nuclei at moderate excitation energies.

The calculation of the number of prefission neutrons which were made by Fraenkel et al.[5] using the code of Dostrovsky et al.[21], shows no "true" prefission neutrons for the fission of ^{226}Ra by 17 MeV protons. We have done a similar calculation for fission of ^{226}Ra by 12 MeV protons, using an improved evaporation program of Hillman and Eyal[22]. This program takes into account angular momenta in the entrance and exit channels, and calculates transition probabilities based on the optical model, and fission probability according to Bohr and Wheeler[23]. The level density formula of Gilbert and Cameron[24] was used in the calculation. Our results are in agreement with the results of Ref. (5), and confirm the conclusion that the

... r of "true" prefission neutrons is almost zero.

The average number of prefission neutrons can also be estimated from the results of Konecny et al.[2] for Γ_f/Γ_n of the Ac isotopes, using the following equation:

$$\bar{\nu}_b = \frac{(\Gamma_f/\Gamma_T)_{226_{Ac}}}{(\Gamma_f/\Gamma_n)_{227_{Ac}} + (\Gamma_f/\Gamma_T)_{226_{Ac}}} \qquad (2)$$

By extrapolating the results for Γ_f/Γ_n of ^{227}Ac to an excitation energy of 17 MeV, and taking the value of $(\Gamma_f/\Gamma_T)_{226_{Ac}}$ at an average excitation energy of 8.5 MeV, and averaging between the two fission modes, we obtain $\bar{\nu}_b$ = 0.09±0.03 n/fission, for fission of ^{226}Ra by 12 MeV protons.

The fact that the average number of "true" prefission neutrons is almost zero, supports the conclusion of Konecny et al.[2] and Weber et al.[3] that the two fission modes which are observed in the fission of nuclei in the Ra region originate from the same nucleus.

Acknowledgements

The authors wish to thank Dr. A. Gavron and Dr. A. Wolf for their valuable help in the experiment, and in the data analysis, and to Dr. E. Cheifetz for many useful discussions. The authors also thank the Weizmann Institute Tandem staff for operating the accelerator and solving many technical problems, and to Prof. Dr. H.J. Specht and Dr. E. Konecny for the Ra targets.

Table 1. The average number of neutrons/sr per fission event N, and the average kinetic energy in the laboratory frame $\bar{\eta}$, at 0° and 90° to the fission axis. Our results are for the energy range 0.5-10.0 MeV. The error due to velocity dispersion is approximately 5%.

	^{226}Ra - p our result	^{252}Cf our results	^{252}Cf Bowman et al.[9]
N(0°)(n/fission/sr)	0.65	0.72	0.8
N(90°)(n/fission/sr)	0.13	0.12	0.12
N(0°)/N(90°)	5.0	6.0	6.6
$\bar{\eta}$(0°) (MeV)	2.75	2.85	3.00
$\bar{\eta}$(90°) (MeV)	2.26	2.16	2.10

References

1) R.C. Jensen and A.W. Fairhall, Phys. Rev. 109, 942 (1958).

2) E. Konecny, H.J. Specht, J. Weber, in Proceedings of the Third Symposium on the Physics and Chemistry of Fission, Rochester, 1973 (IAEA, Vienna 1974) p. 3, Vol. II.

3) J. Weber, H.C. Britt, A. Gavron, E. Konecny and J.B. Wilhelmy, Phys. Rev. C 13, 2413 (1976).

4) E. Konecny and H.W. Schmitt, Phys. Rev. 172, 1213 (1968).

5) Z. Fraenkel, I. Mayk, J.P. Unik, A.J. Gorski and W.D. Loveland, Phys. Rev. C 12, 1809 (1975).

6) H.W. Schmitt, W.E. Kiker and C.W. Williams, Phys. Rev. 137, B837 (1965).

7) J.M. Alexander and M.F. Gazdick, Phys. Rev. 120, 874 (1960).

8) A. Gavron, Nucl. Instrum. Methods 115, 99 (1974).

9) H.R. Bowman, S.G. Thompson, J.C.D. Milton and W.J. Swiatecki, Phys. Rev. 126, 2120 (1962).

10) A. Gavron and Z. Fraenkel, Phys. Rev. C 9, 632 (1974).

11) E. Cheifetz, Z. Fraenkel, J. Galin, M. Lefort, J. Peter and X. Tarrago, Phys. Rev. C 2, 256 (1970).

12) A. Gavron, Nucl. Instrum. Methods 115, 93 (1974).

13) D.G. Perry and A.W. Fairhall, Phys. Rev. C 4, 977 (1971).

14) F. Plasil, R.L. Ferguson, H.W. Schmitt, in Proceedings of the Second Symposium on the Physics and Chemistry of Fission, Vienna, 1969 (IAEA, Vienna, 1969), p. 505.

15) A. Volpi and K.G. Porgess, Phys. Rev. C 1, 683 (1970).

16) H. Nifenecker, C. Signarbieux, R. Babinet and J. Poitou, in Proceedings of the Third Symposium on the Physics and Chemistry of Fission, Rochester 1973 (IAEA, Vienna, 1974) p. 117, Vol. II.

17) T. Ericson and V. Strutinsky, Nucl. Phys. 8, 284 (1958).

18) A. Wolf and E. Cheifetz, Phys. Rev. C 13, 1952 (1976)

19) H.C. Britt, H.E. Wegner and J.C. Gursky, Phys. Rev. 129, 2239 (1963)

20) J.R. Nix, W.J. Swiatecki, Nucl. Phys. 71, 1 (1965).

21) I. Dostrovsky, Z Fraenkel, and P. Rabinovitch, in Proceedings of the Second United Nations International Conference on the Peaceful Uses of Atomic Energy (U.N., Geneva, 1958), Vol. 15, p. 301.

22) M. Hillman and Y. Eyal, in Proceedings of the European Conference on Nuclear Physics with Heavy Ions, (Caen, 1976) p. 109.

23) N. Bohr and J.A. Wheeler, Phys. Rev. 56, 426 (1939).

24) A. Gilbert and A.G.W. Cameron, Canadian Journal of Physics 43, 1446 (1965).

Figure Captions

Fig. 1. The geometrical arrangement of the experiment. The beam direction is perpendicular to the plane of detectors.

Fig. 2. The block diagram of the electronic system. The units described by dashed lines were used with the liquid scintillator NE 213

Fig. 3. The time-of-flight spectrum at 0° and 90° to the fission axis.

Fig. 4. The rise-time distribution for 5" diam x 2" thick liquid scintillators NE 213. The amplifier used was an Ortec model 460. The lower level energy discrimination was set at 200 keV neutron energy.

Fig. 5. The effective efficiency for neutron detection with the plastic scintillator NE 102, at 0°(O) and 90°(•) to the fission axis. The dashed line is the intrinsic efficiency of the scintillator, calculated by assuming single scattering of the neutrons in the scintillator.

Fig. 6. The contour plot of the fission yield $Y(A,E_k)$ as a function of the prompt fragment mass A, and total kinetic energy E_k. The spacing of the contours is 1.5×10^3 events. The dashed line shows the separation between the symmetric and asymmetric fission modes.

Fig. 7. The average number of postfission neutrons per fragment $\bar{\nu}_a(A)$, as a function of the prompt fragment mass A, and the mass distribution Y(A) shown by the full line. Where the statistical errors are not given they are too small to be shown.

Fig. 8. The average number of postfission neutrons per fragment $\bar{\nu}_a(E_k)$, as a function of the prompt total kinetic energy E_k, and the total kinetic energy distribution $Y(E_k)$ shown by the full line. Where the statistical errors are not given they are too small to be shown.

Fig. 9. The laboratory neutron spectra at 0°(0) and 90°(•) to the fission axis for ^{226}Ra + 12 MeV protons and the spontaneous fission of ^{252}Cf.

Fig. 10. The contour plot of the average number of postfission neutrons per fragment $\bar{\nu}_a(A,E_k)$, as a function of the prompt fragment mass A, and the total kinetic energy E_k. The lowest contour of the fission yield $Y(A,E_k)$ is shown for reference by the dashed line.

Fig. 11. The average derivative of $\bar{\nu}_a$ with respect to E_k, $\frac{\partial\bar{\nu}_a}{\partial E_k}$ (A) as a function of the prompt fragment mass A. The mass distribution in arbitrary units is shown as a dashed line for reference.

Fig. 12. The postfission neutron spectrum $N_{c.m}(\eta)$ in the c.m. frame of the fragment

Fig. 13. The average kinetic energy of the postfission neutrons $\bar{\eta}_a(A)$ as a function of the prompt fragment mass A. The mass distribution is shown as a full line for reference. The errors in $\bar{\eta}_a$ include the uncertainty in the time-of-flight measurement.

Fig. .. The average number of prefission neutrons per fission $\bar{\nu}_b(A)$ as a function of the prompt fragment mass A (the results were symmetrized with respect to A = 113.5). The mass distribution is shown as a full line for reference.

Fig. 15. The prefission neutron spectrum $N_{c.m.}(\eta)$ in the c.m. frame of the fissionning nucleus.

Fig. 16. The average number of postfission neutrons $\bar{\nu}_a(A)$ as a function of fragment mass A, for the symmetric and the asymmetric modes. The corresponding mass distributions Y(A) are shown as full lines. The statistical errors in $\bar{\nu}_a$ can be inferred from the fluctuations between neighboring points.

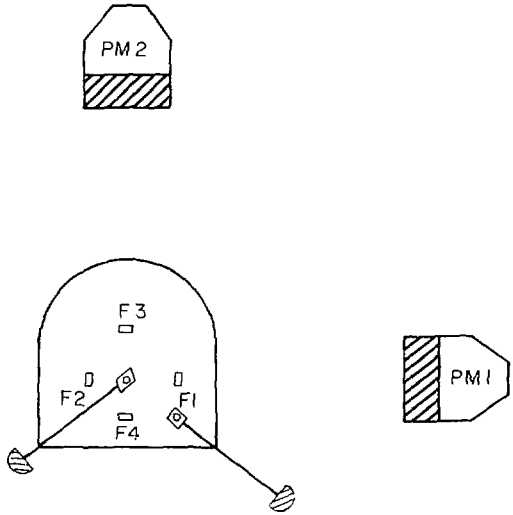

Fig. 1

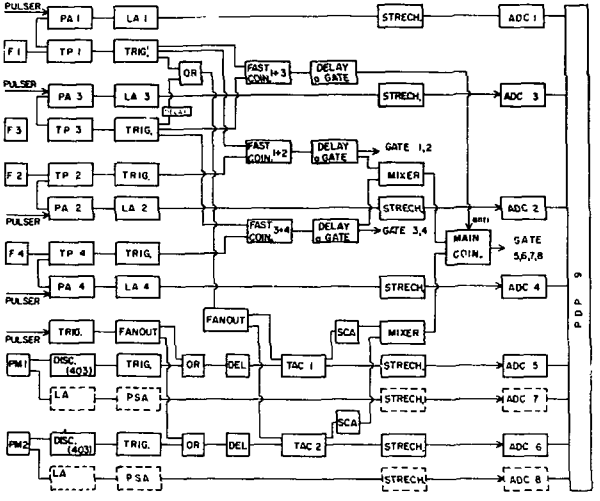
PULSER
PA 1
LA 1
STRECH.
ADC 1
F 1
TP 1
TRIG.
OR
FAST COIN. 1+3
DELAY & GATE
PULSER
PA 3
LA 3
STRECH.
ADC 3
F 3
TP 3
TRIG.
FAST COIN. 1+2
DELAY & GATE
GATE 1,2
F 2
TP 2
TRIG.
MIXER
PULSER
PA 2
LA 2
STRECH.
ADC 2
FAST COIN. 3+4
DELAY & GATE
GATE 3,4
F 4
TP 4
TRIG.
MAIN COIN.
GATE 5,6,7,8
PULSER
PA 4
LA 4
STRECH.
ADC 4
FANOUT
PULSER
TRIG.
FANOUT
SCA
MIXER
PM1
DISC. (403)
TRIG.
OR
DEL
TAC 1
STRECH.
ADC 5
LA
PSA
STRECH.
ADC 7
SCA
PM2
DISC. (403)
TRIG.
OR
DEL
TAC 2
STRECH.
ADC 6
LA
PSA
STRECH.
ADC 8
PDP 9

Fig. 2

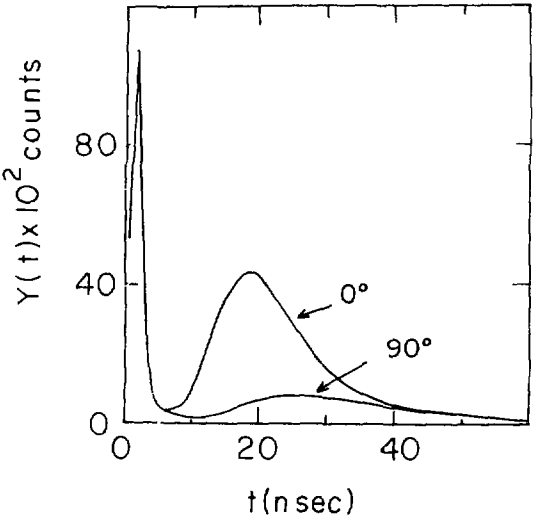

Fig. 5

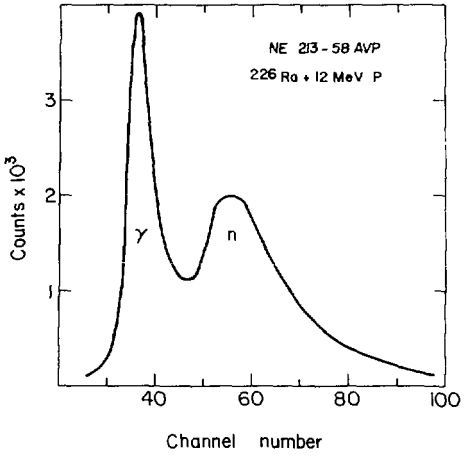
NE 213 - 58 AVP
226 Ra + 12 MeV P
Counts x 10^3
3
2
1
γ
n
40
60
80
100
Channel number

Fig. 4

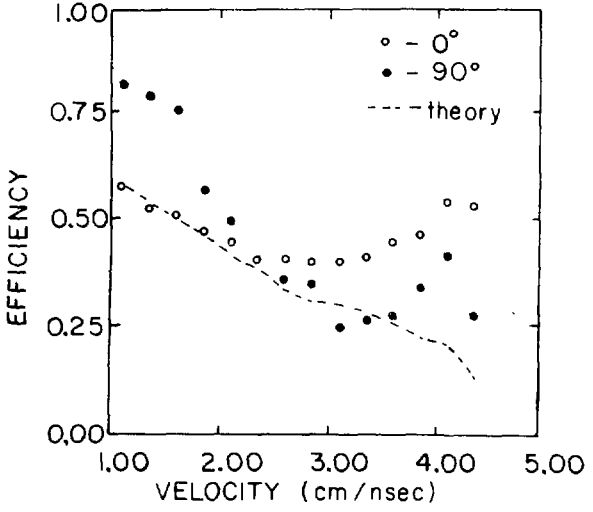
1.00
0.75
0.50
0.25
0.00
EFFICIENCY
1.00
2.00
3.00
4.00
5.00
VELOCITY (cm/nsec)
○ - 0°
● - 90°
---theory

Fig. 5

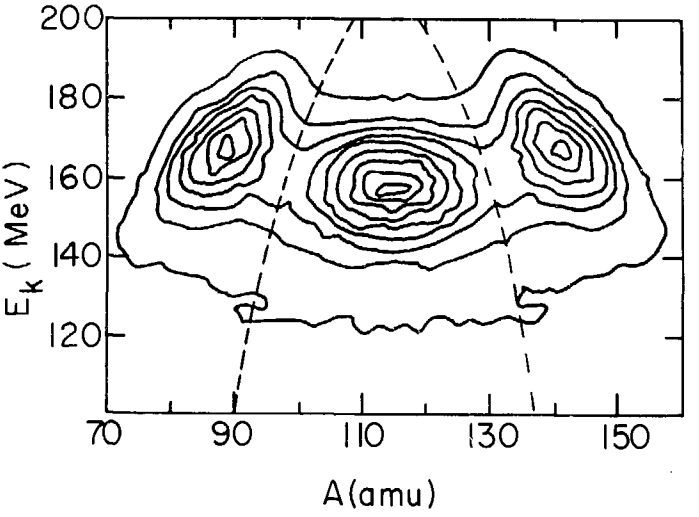

Fig. 6

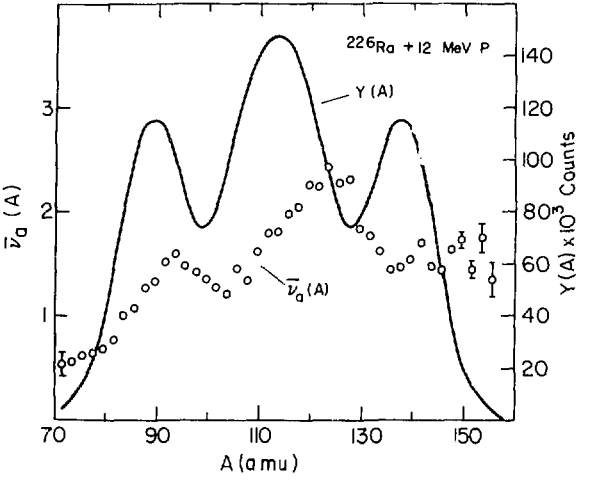
226Ra + 12 MeV P
Y (A)
$\bar{\nu}_a$ (A)
$\bar{\nu}_a$ (A)
Y (A) x 10^3 Counts
A (a mu)
70
90
110
130
150
1
2
3
20
40
60
80
100
120
140

Fig. 7

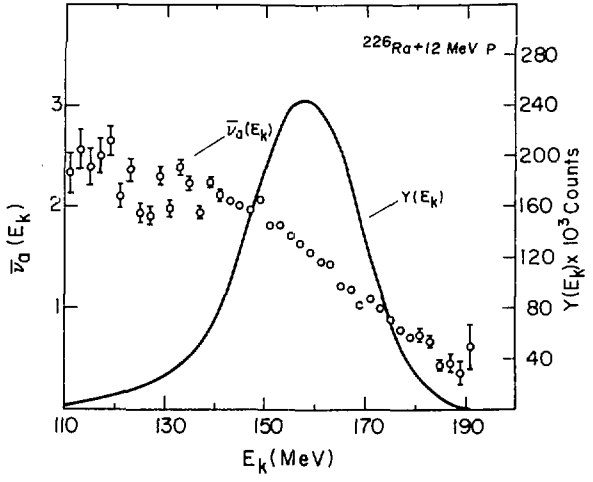
^{226}Ra+12 MeV P
$\bar{\nu}_a(E_k)$
$Y(E_k)$
$\bar{\nu}_a(E_k)$
$Y(E_k)\times 10^3$ Counts
E_k(MeV)
110
130
150
170
190
1
2
3
40
80
120
160
200
240
280

Fig. 8

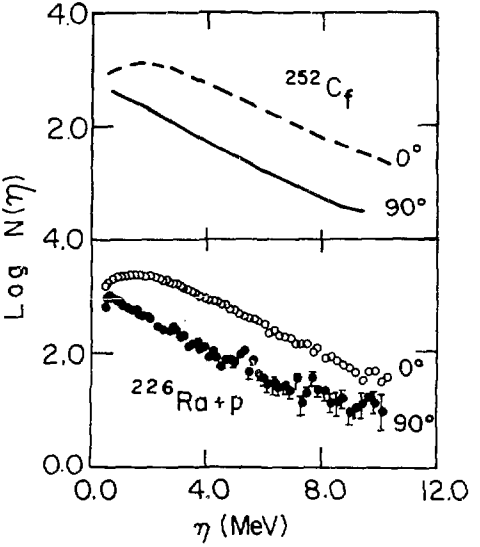

Fig. 9

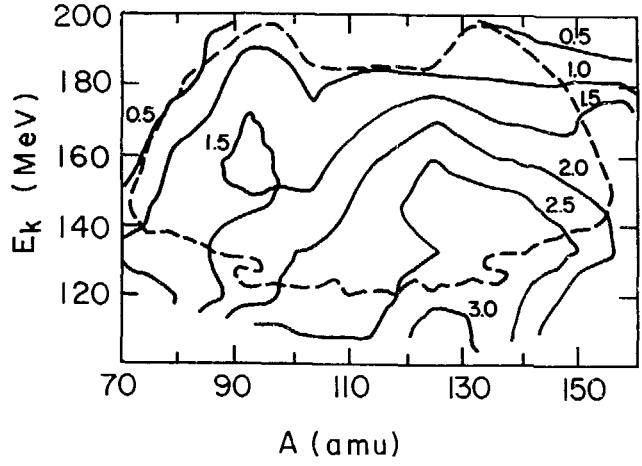
200
180
160
140
120
E_k (MeV)
70
90
110
130
150
A (amu)
0.5
1.0
1.5
2.0
2.5
3.0
0.5
1.5

Fig. 10

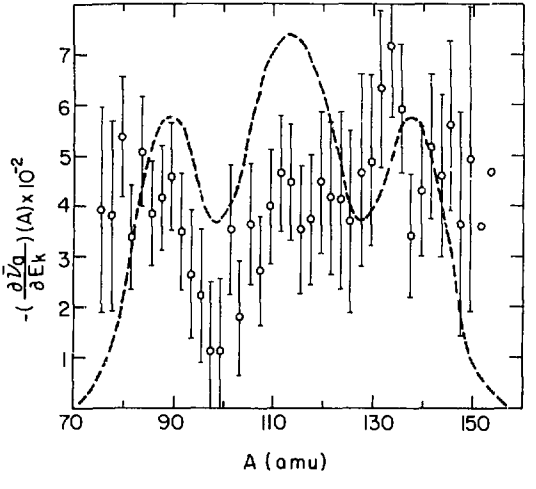
$-\left(\frac{\partial \bar{\nu}_a}{\partial E_k}\right)(A) \times 10^{-2}$
1
2
3
4
5
6
7
70
90
110
130
150
A (amu)

Fig 11

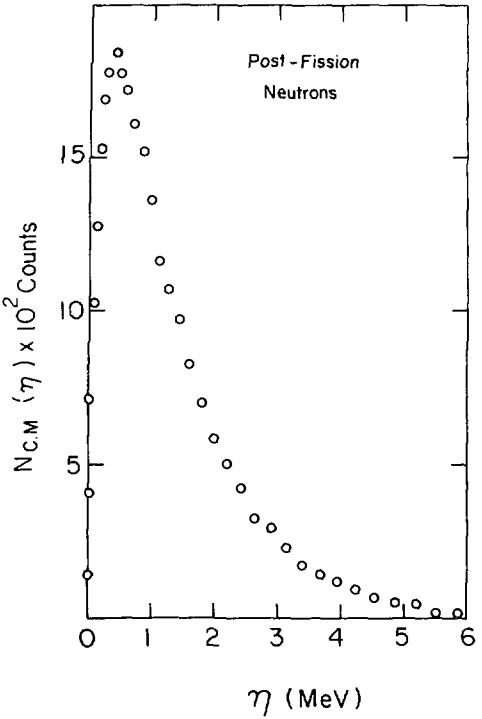
Post-Fission
Neutrons
15
10
5
0
1
2
3
4
5
6
$N_{C.M}(\eta) \times 10^2$ Counts
η (MeV)

Fig. 12

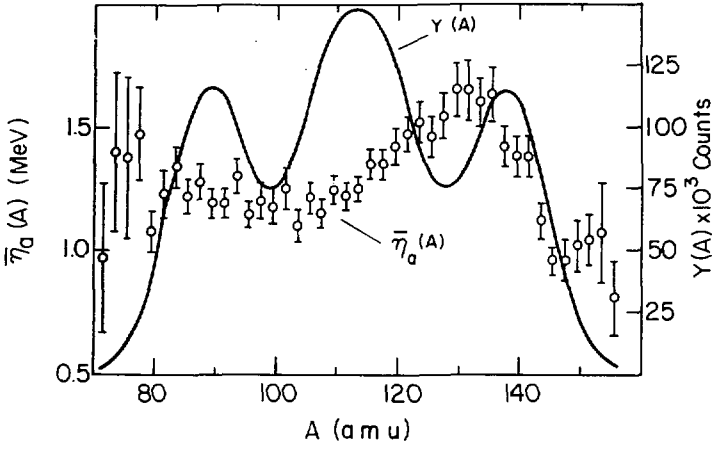
Y (A)
$\bar{\eta}_a$ (A)
$\bar{\eta}_a$ (A) (MeV)
Y(A) x10^3 Counts
A (a m u)
0.5
1.0
1.5
80
100
120
140
125
100
75
50
25

Fig. 13

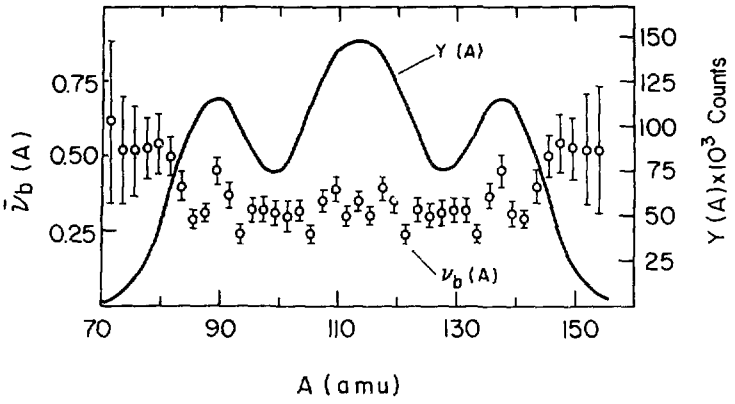
Y (A)
ν_b (A)
$\bar{\nu}_b$ (A)
0.75
0.50
0.25
150
125
100
75
50
25
Y (A)x10^3 Counts
70
90
110
130
150
A (amu)

Fig. 14

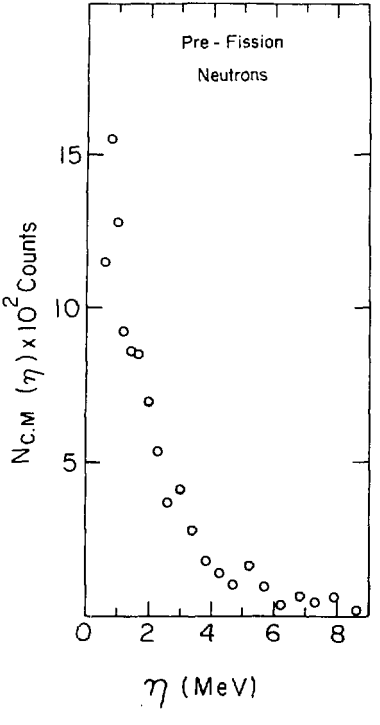
Pre - Fission
Neutrons
15
10
5
0
2
4
6
8
$N_{C.M}$ (η) x 10^2 Counts
η (MeV)

Fig. 15

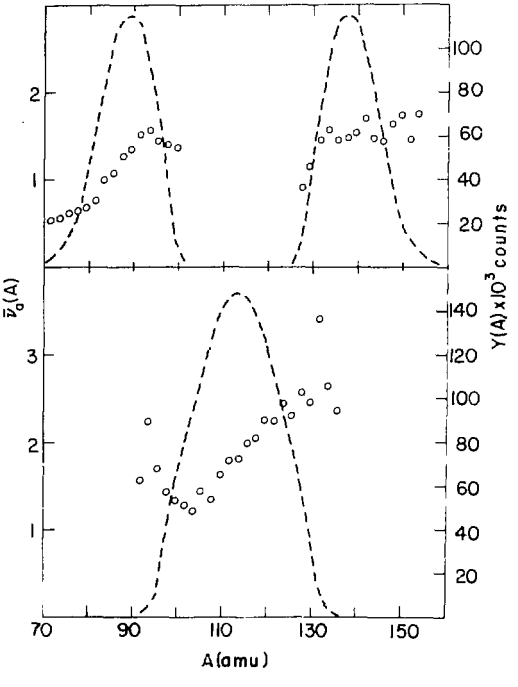
$\bar{\nu}_0(A)$
Y(A)x10^3 counts
A(amu)
70
90
110
130
150
1
2
3
20
40
60
80
100
120
140
d
p

Fig. 16